



Wake-based unsteady modeling of the aquatic beetle *Dytiscus marginalis*

Robert W. Whittlesey

Graduate Aerospace Laboratories of the California Institute of Technology, Pasadena, CA 91125, USA

ARTICLE INFO

Article history:

Received 20 March 2011

Received in revised form

19 June 2011

Accepted 2 August 2011

Available online 6 September 2011

Keywords:

Swimming

Vortex modeling

Insects

Vortex rings

Efficiency

ABSTRACT

Dytiscus marginalis simultaneously uses its hind legs to propel itself through the water. Previous work has suggested that use of synchronized leg motions, such as that used by *D. marginalis*, allows it to swim with higher hydrodynamic efficiency than similarly sized insects that alternate their legs during swimming. A model is developed based on the generation of vortices in the wake to calculate the relative efficiency of synchronized-leg-swimming kinematics compared to alternating-leg-swimming kinematics. The model agrees well with measured values of swimming speeds during steady state and predicts an overall hydrodynamic swimming efficiency of 18% for synchronized-leg-swimming. Additionally, synchronized-leg swimming is calculated to be 39% more hydrodynamically efficient than alternating-leg-swimming kinematics, thus verifying previous suggestions of greater hydrodynamic efficiency in *D. marginalis* based on swimming observation.

© 2011 Elsevier Ltd. All rights reserved.

1. Introduction

Members of the family *Dytiscidae* are aquatic predators of the insect world. Adults have streamlined bodies and use powerful hind legs to propel themselves through the water. Many species of *Dytiscidae* simultaneously use both legs during the power stroke, whereas the hind legs of other aquatic insects, such as *Hydrophilus piceus*, are out of phase. Hughes (1958) suggests that *D. marginalis* are aquatically more efficient on the basis of their leg movements and by observation of the unsuitability of *D. marginalis* to terrestrial locomotion. The leg coordination of *H. piceus* is very similar to the patterns that land-based insects use (with alternating leg movements) and thus there is speculation that its leg movements may represent a more basal state whereas the leg coordination of *Dytiscidae* may indicate a more developed swimming coordination. Thus it appears as though the synchronous leg movements uniquely sets some members of *Dytiscidae* apart from other insects and is believed to be an adaptation uniquely developed for its role as an aquatic predator. To test these concepts, a model is developed to comparatively study alternating- versus synchronized-leg-swimming kinematics and their impact on swimming speed and hydrodynamic efficiency. The model will focus on one insect species and within the model its swimming stroke will be changed to determine the swimming performance. *Dytiscus marginalis* was chosen for study due to the number of measurements already available on the swimming characteristics and kinematics of this species.

2. Modeling

2.1. Dimensions and kinematics

Whereas *D. marginalis* swims throughout the depths of the water in which it inhabits, the model restricts motion purely to the two dimensions of forward and lateral swimming motion. Thus any pitching or diving motions will be neglected. The basic leg motion of an insect from the *Dytiscidae* family is shown in Fig. 1(a). During the power stroke, the tips of the hind legs begin anterior of the coxae and throughout the stroke the legs remain relatively straight as the insect powers itself forward. At the conclusion of the power stroke, the legs are now pointing nearly straight downstream. For the recovery stroke, the legs bend at the femoro-tibial joint allowing the more distal tibia and tarsus (with their associated swimming hairs) to be streamlined against the direction of travel, minimizing their drag (Nachtigall, 1980).

2.1.1. Leg kinematics

For the kinematics of the swimming, the model uses leg-tip plottings from Hughes (1958) as shown in Fig. 1(b). These kinematics show the beat frequency of paddling to be approximately 3 Hz and the model uses exactly 3 Hz for its simulation. During motion capture, the insect was turning slightly to the left which explains the asymmetry in the leg motions. The right hind leg is assumed to follow a regular path and it is assumed that the insect was controlling the stroke path on the left hind leg to execute the left turn. This is supported by Fig. 1(a) where the transition from the power to recovery stroke leaves the hind leg tip near the medial line of the insect body which is in agreement with the right hind leg path

E-mail address: whittlesey@caltech.edu

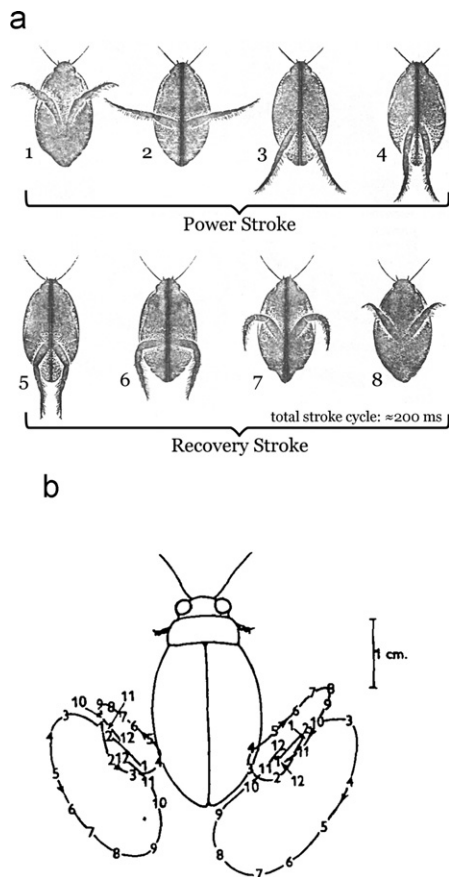


Fig. 1. Leg motions insects from the *Dytiscidae* family: (a) hind leg motions of *Acilius sulcatus*, a member of the *Dytiscidae* family, showing the hind leg positions during the power stroke and recovery stroke. Only the hind legs are shown in these photos. From [Nachtigall \(1980\)](#). (b) Leg kinematics of *D. marginalis* from [Hughes \(1958\)](#). Each numbered location corresponds to the position of leg tip for the middle and hind leg on a frame during motion capture (30 frames per second). The insect was turning to the left and hence the asymmetry in the leg motions.

in [Fig. 1\(b\)](#). Furthermore, for *D. marginalis* it is primarily the hind legs which are responsible for the majority of propulsion, as the middle legs only play a regular part in swimming motion under rapid swimming and even then only to stabilize the body during the recovery stroke ([Hughes, 1958](#)). Because of this, only the movement of the hind legs will be considered in this model. To distinguish between the power and recovery strokes, the maximum anterior point of the leg-tip trajectory is chosen as the onset of the power stroke and the maximum medial point of the leg-tip trajectory as the onset of the recovery stroke. The leg-tip traces from [Fig. 1\(b\)](#) were digitized to a path which is spline fit to obtain a smooth curve and yield a finer resolution of leg motion for later numerical calculations.

2.1.2. Leg assumptions

For the modeling of the hind legs, a straight line from the hind coxae to the leg-tip is used and the legs are considered to be flat plates. The location of the hind coxae is given by photos of *D. marginalis* in [Nachtigall \(1980\)](#). The straight line assumption for the legs is a reasonable approximation particularly during the power stroke as seen in [Fig. 1\(a\)](#). However, during the recovery stroke, the legs bend at the femoro-tibial joint and have a streamlined recovery. The validity of this assumption will be addressed in [Section 4](#). The width of the leg is assumed to take two values: a larger value during the power stroke to represent the fanning of the swimming hairs dorsally and ventrally and a smaller value during recovery to represent solely the width of the

leg, as now the hairs are folded down. [Hughes \(1958\)](#) shows that the tarsus and tibia are flattened and during the power stroke the cross-section of the legs is primarily perpendicular to the leg motion, maximizing the area of their legs, whereas during the recovery stroke the tibia and tarsus sections rotate as to minimize their projected area into the direction of leg motion. From [Nachtigall \(1980\)](#) an estimate for the leg width during the power stroke is determined using an image of *Acilius sulcatus*, and this results in the leg width alone to be approximately 1.3 mm. During recovery it is assumed that the projected width of the leg in the direction of motion is one half of its width during the power stroke based on [Hughes \(1958\)](#), giving a recovery stroke width of 0.65 mm. Furthermore, [Nachtigall \(1980\)](#) states that 68% of the force on the leg of *Acilius* is from its hairs. The force generated by the leg motion is assumed to be proportional to the area and an effective width for the leg during the power stroke is calculated to be 4.2 mm, based on the width of the leg alone. The sensitivity of the results to these values and assumptions is given in [Section 3.1](#) and discussed in [Section 4](#).

2.1.3. Insect body

The insect body is approximated as an ellipsoid using [Fig. 1\(b\)](#) for the dorsal dimensions and the depth of the body from [Nachtigall and Bilo \(1974\)](#). The ellipsoid shape ignores some of the features that make the body of *D. marginalis* streamlined such as its largest body depth being just before the middle of the body ([Nachtigall and Bilo, 1974](#)). However by making this assumption the following model is able to leverage existing results for the hydrodynamics of ellipsoidal bodies. This gives the volume of the beetle body as well as approximations to the accelerations of the body. The insect mass is approximated from measurements in [Giovannia et al. \(1999\)](#) of 37 adult *D. marginalis* beetles who found their live weight to have mean of 2.2 g.

2.2. Wake-based model

2.2.1. Equations of motion

Using Newton's second law, the forces and moments on the insect are related to the accelerations of the insect as

$$\sum F_x = \tilde{m} a_x \quad (1a)$$

$$\sum F_y = \tilde{m} a_y \quad (1b)$$

$$\sum M_z = \tilde{I} \alpha_z \quad (1c)$$

where F_x and F_y are the hydrodynamic forces on the insect in the x and y directions respectively, M_z is the moment on the body around the z axis, \tilde{m} is the combined true mass and added mass of the insect body, a_x and a_y are the lateral accelerations in the x and y directions, respectively, \tilde{I} is the combined true mass moment of inertia and added mass moment of inertia, and α_z is the angular acceleration in the z direction. The model assumes that the insect is moving in the positive y -direction with x being the lateral direction of movement leaving z to be the vertical direction out of the page, as shown in [Fig. 2](#).

The combined true mass and added mass of the body can be found by

$$\tilde{m} = m_{true} + \kappa_{yy} V_{body} \rho \quad (2)$$

where m_{true} is the measured weight of the insect from [Giovannia et al. \(1999\)](#), κ_{yy} is the added mass coefficient for an ellipsoid-approximation of the insect body shape given by equations in [Brennen \(1982\)](#) for an ellipsoid moving along its largest semi-axis, V_{body} is the volume of the ellipsoid-approximation of the

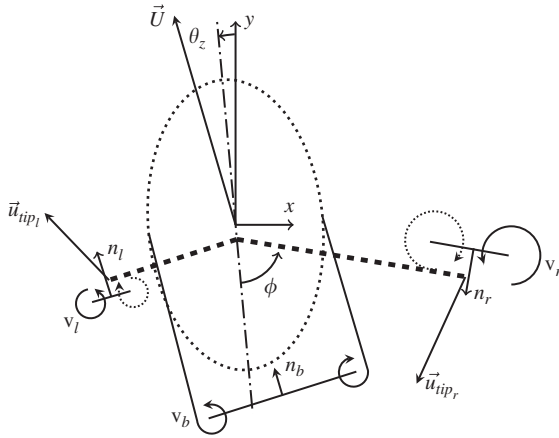


Fig. 2. Schematic showing the wake structure and orientation of the insect. The insect body is given as the dotted ellipse and the legs are given as thick dashed lines. The left leg is in the midst of a recovery stroke and forms a vortex denoted v_l with normal vector \mathbf{n}_l . The left leg-tip velocity is denoted as the vector $\vec{u}_{tip,l}$. The densely dotted, opposite-signed vortex represents the bound vortex on the leg. The right leg is in the midst of a power stroke and forms a vortex denoted v_r with normal vector \mathbf{n}_r . The right leg-tip velocity is denoted as the vector $\vec{u}_{tip,r}$. The body is assumed to shed a vortex ring and is denoted v_b in this schematic. The angle a leg makes with the medial line of the insect is denoted by the angle ϕ and the angle the body makes with the y -axis is denoted as the angle θ . The velocity of the body is given by \vec{U} and in the time averaged sense is assumed to be aligned with the y -axis.

insect body, and ρ is the fluid density (1 g cm^{-3}). Similarly, the combined true mass moment of inertia and added mass moment of inertia is defined as

$$\tilde{I} = m_{true} \frac{l_b^2 + w_b^2}{20} + \kappa_z V_{body} \rho \frac{l_b^2 + w_b^2}{20} \quad (3)$$

where l_b and w_b are the insect's body length and body width, respectively, and κ_z is the added mass coefficient for an ellipsoid rotating around its smallest axis (Brennen, 1982).

2.2.2. Insect wake structure

Since the beetle is only in horizontal motion, any force due to gravity or buoyancy does not act in this plane. Thus only the hydrodynamic forces on the insect body and its legs remain. To calculate the forces generated by the body and movements of the legs, the model assumes that in the wake of the insect there will be vortices and that from these vortices alone the resulting forces on the insect and ultimately the motion of the insect are calculated. The wake structure for *D. marginalis* is defined as shown in Fig. 2 where there are three vortical structures used in the model. The first structure is the vortex ring v_b which represents the vorticity shed from the insect body as it swims. It is expected that this is a complicated structure based on the wake of a sphere (Achenbach, 1974), however this simplified model will assume that there is only a single vortex ring produced. This is a reasonable assumption as the more complicated structures in a wake develop downstream of the body and since the effect of a vortex goes as r^{-2} , where r is the distance from the vortex element to the point of interest, the effect of any vortex elements in the wake diminishes quickly. The plane of this vortex ring will be perpendicular to the direction of motion and will have area equal to the elliptic cross-section in the middle of the insect body.

The other two vortex structures in the model are vortical structures created by the motions of the legs as shown in Fig. 2. Based on the experimental results of Kim (2010), who experimentally studied paddling motions using flat plates and three-dimensional velocimetry methods, the vortex created at the tip of a flat plate will have an equal and opposite vortex that is bound to

the leg itself. Thus in the model it is assumed that the hind leg's combined bound vorticity and tip vortex can be modeled as a single vortex ring, denoted in the figure as v_l and v_r for the left and right vortex rings, respectively. Each vortex ring is assumed to be centered at the leg tip, to have diameter equal to the width of the leg, and to always be parallel to the leg. This last assumption is reasonable during the bulk of a stroke, however at the end of the stroke the accumulated circulation will become a shed vortex and this model does not include the effects of shed vortices. Furthermore, the leg does change width during the full stroke cycle as mentioned in Section 2.1.2, however it is assumed that the leg width is constant during each stage of the stroke cycle and that the change in width is instantaneous.

2.2.3. Vortex forces

The impulse of a vortex ring surrounded by irrotational flow is given by Thomson (1883):

$$\vec{P} = \rho \Gamma S \mathbf{n} \quad (4)$$

where P is the impulse of the vortex ring, ρ is the density of the fluid, Γ is the circulation of the vortex ring, S is the area of the vortex ring (e.g. $S = \pi R^2$ for a circular ring of radius R), and \mathbf{n} is the unit normal to the plane of the vortex ring. The assumption of irrotational flow surrounding the vortex ring is reasonable for our insect as it is further assumed that the insect is freely swimming in quiescent flow. In reality there will be vortex interactions between the vortices shed from each hind leg and from the body, however the model assumes that those interactions are negligible. This assumption is valid because, as mentioned previously, the effect of a vortex goes as r^{-2} and thus the effect of any vortex elements after shedding (whether interacting or not) quickly becomes of negligible significance.

Using Eq. (4), the force required to produce the vortex ring and hence the magnitude of the reacting force on the insect is obtained as

$$\vec{F} = \frac{d\vec{P}}{dt} = \rho \frac{d}{dt} (\Gamma S) \mathbf{n} \quad (5)$$

where the model assumes that the density of the fluid is constant and that $d\mathbf{n}/dt \approx 0$. What remains is a relation for the force that is dependent on the time rate of change of the product of the circulation and the area of the vortex ring. The area, S , can be estimated from assumptions for the dimensions of the vortex ring as given in Section 2.2.2. Furthermore, the circulation, Γ , can be estimated using the flux of vorticity in the boundary layer as

$$\frac{d\Gamma}{dt} = \frac{1}{2} u^2 \quad (6)$$

where u is the flow velocity external to the boundary layer, based on page 68 of Rosenhead (1963). For modeling the three vortex rings in this model, the external flow velocity, u , is chosen depending on the surface generating the vorticity as the body and each leg will experience different local velocities.

The estimated vorticity flux is a first-order approximation and does not include such effects as the shape of the body, however it is assumed that the boundary layer thickness is much smaller than the radius of curvature of the surface as the Reynolds number of the insect swimming is assumed to be high. Furthermore, Eq. (6) is derived from flow parallel to a surface and this is suitable for this model as the flow along the body of the insect will be predominantly parallel to the body surface (with the exception of the most anterior and posterior ends of the body) and it is assumed that there will be significant span-wise flow along that legs that will be parallel to the legs' surface (Ringette et al., 2007).

The force from the body vortex, v_b , on the insect can be obtained through Eqs. (5) and (6). Using the assumptions given in Section 2.2.2 and choosing the body velocity as the external flow velocity in Eq. (6) yields

$$\vec{F}_{v_b} = -\pi\rho\frac{1}{2}|\vec{U}|^2\frac{w_b d_b}{4}\mathbf{n}_b = -\frac{\pi\rho w_b d_b}{8}|\vec{U}|^2\frac{\vec{U}}{|\vec{U}|} \quad (7)$$

where $||$ denotes the norm of a vector, \vec{U} is the velocity of the insect body's center of mass, and d_b is the depth of the insect body. Similarly applying Eqs. (5) and (6) to the movement of the legs and using the leg-tip velocity as the external flow velocity in Eq. (6), a relation is obtained for the force from the leg vortex rings, v_l and v_r , on the insect as

$$\vec{F}_{v_i} = -\frac{\pi\rho w_l^2}{8}|\vec{u}_{tip_i}|^2\mathbf{n}_i \quad (8)$$

where i is an index with values of l and r , \vec{u}_{tip_i} is the leg-tip velocity, and w_l is the leg width. Note that only ρ in Eq. (8) is assumed constant with all other terms being a function of time as well as the swimming kinematics.

2.2.4. Hydrodynamic efficiency

The efficiency is generally defined as the amount of useful power relative to the power to produce that useful work. Thus the hydrodynamic efficiency of *D. marginalis* will be defined as the power used to produce forward motion relative to the power in the entire system. This is written as

$$\eta = \frac{\langle [(\vec{F}_{v_l})_y + (\vec{F}_{v_r})_y]U_y \rangle}{\langle |\vec{F}_{v_l}||\vec{u}_{tip_l}| \rangle + \langle |\vec{F}_{v_r}||\vec{u}_{tip_r}| \rangle + \langle M_z\omega_z \rangle} \quad (9)$$

where $\langle \rangle$ denotes time averaging, subscript y defines the y -component of a vector, and ω_z is the angular velocity of the body. From this definition, an insect that produces only forces in the y -direction will be much more efficient than an insect that produces forces in the x -direction or rotates its body. The time averaging only includes values at steady state. Because the beetle will be swimming freely at steady state the mean of Eq. (1) will be zero, however the numerator in Eq. (9) explicitly ignores the force from the body vortex as it only impedes swimming and is not considered contributing to "useful work," thus the numerator in Eq. (9) will be non-zero.

2.2.5. Simulation

The initial conditions for simulating the swimming performance of *D. marginalis* are that the body velocity and acceleration are zero and the body angular velocity and angular position have values of $\omega_z = \omega_{z,0}$ and $\theta_z = \theta_{z,0}$. Eqs. (1)–(3), (7) and (8) are solved at each time step and time-marched using the Euler method. There are 100 points used to describe the leg kinematics and based on the beat frequency of swimming the time step for time marching is 1/300th of a second. For convergence testing, the time-step size was reduced by a factor of five and no significant change in the results was observed. The insect reaches steady-state swimming after approximately 3 s and continues to swim freely until the center of mass of the insect reaches $y=60$ cm, which takes approximately 10 s in the simulation. The last 3 s (900 data points) are used in averaging and calculating the swimming efficiency.

Two cases are simulated: one case where the leg kinematics are synchronized and the other where the left and right leg motions are alternating (180° out of phase). For the synchronized-leg-swimming kinematics, the starting conditions are such that $\omega_{z,0}, \theta_{z,0} = 0$. For

the alternating-leg-swimming kinematics, the starting conditions for $\omega_{z,0}$ and $\theta_{z,0}$ are such that $\lim_{t \rightarrow \infty} (\langle \omega_z \rangle, \langle \theta_z \rangle) \rightarrow 0$. This could alternatively be achieved by setting $\omega_{z,0}, \theta_{z,0} = 0$ and altering the initial position of the legs at $t=0^1$ but in practice setting $\omega_{z,0}, \theta_{z,0} \neq 0$ proved more effective to ensure the insect swam straight.

3. Results

A plot of the trajectory of the insect head from the model is shown in Fig. 3(a) for each swimming style. A movie of the insect swimming along this trajectory is available in the online supplementary material (Video S1). The synchronized-leg-swimming kinematics yield a straight line in the y -direction, as expected due to the moment and lateral velocity being identically zero (cf. Fig. 4(b)). However, the alternating-leg swimming clearly shows a transient during the initial swimming motion as the spatial wavelength of oscillations increases. Additionally, this transient causes the insect to have, on average, a non-zero lateral (x) displacement which is a function of the starting leg position and initial conditions for the angular velocity and position. The start-up process is also available as a movie in the supplemental material (Video S2). Fig. 3(b) is from Hughes (1958) and shows two head trackings of a *H. piceus* beetle, which uses alternating-leg-swimming kinematics to swim. Comparing the modeled alternating-leg-kinematics *D. marginalis* and the observations of *H. piceus* both show a rotational oscillation that is synchronized to the leg beat frequency.

Supplementary material related to this article can be found online at doi:10.1016/j.jtbi.2011.08.005.

Fig. 4 shows the vortex forces from the legs as well as translational and angular accelerations during steady state swimming. A movie of the simulated insects swimming during the same time as these plots is available as online supplementary material (Video S3). Fig. 4(a) shows the magnitude of the force from the vortex on the body due to the leg vortices. From this plot, the vortex force magnitude during the power stroke is shown to be at least one order of magnitude greater than during the recovery stroke. Thus the influence of the stroke recovery is minimal relative to the power stroke in this model. Using Eq. (8) the only terms that change in magnitude are w_l and $|\vec{u}_{tip_i}|$. However, $|\vec{u}_{tip_i}|$ is always $\mathcal{O}(10)$ cm s⁻¹ whereas w_l varies between $\mathcal{O}(10^{-1})$ and $\mathcal{O}(10^{-2})$ cm, hence explaining the significant difference between the forces of the power and recovery strokes.

Supplementary material related to this article can be found online at doi:10.1016/j.jtbi.2011.08.005.

Fig. 4(b) compares accelerations between the alternating- and synchronized-leg-swimming kinematics, with the values over-marked by \sim indicating the alternating-leg-swimming kinematics and unmarked values the synchronized-leg-swimming kinematics. In particular, a_y reaches a peak during the power stroke that is over twice as large as the peak of \tilde{a}_y , however \tilde{a}_y is sustained above 0 for more of the total stroke than a_y due to the alternating leg motions. Also due to the alternating of legs, when the left leg conducts a power stroke (from time ≈ 4 –4.17 s) there is a negative \tilde{a}_z (to turn the insect clockwise) and a negative \tilde{a}_x which pulls the insect to the left. This is then compensated for by the reverse occurring during the right leg's power stroke during the rest of the stroke cycle.

Fig. 4(c) shows the velocities of the insect. For the synchronized-leg-swimming kinematics, the insect experiences significant oscillations of its forward velocity as the peak-to-peak amplitude of U_y is 1.75 cm s⁻¹. In contrast, the alternating-leg-swimming insect has a

¹ For example: starting the legs mid-way through their stroke appears to compensate for $\omega_{z,0}, \theta_{z,0} = 0$ whereas if the legs are just at the beginning of a stroke, then $\omega_{z,0}, \theta_{z,0} \neq 0$ to ensure the insect swims straight.

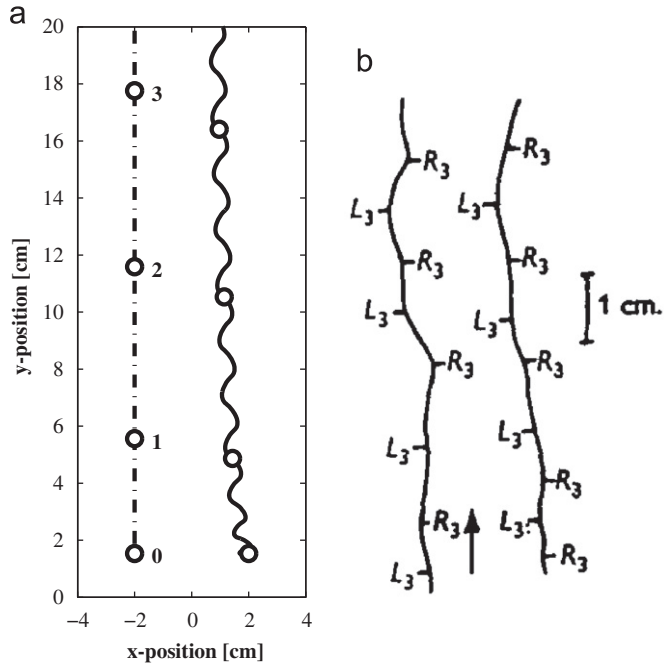


Fig. 3. Head trajectories during swimming for simulation of *D. marginalis* and observation of *Hydrophilus piceus* from Hughes (1958): (a) plot of the trajectory of the insect head during the start of swimming. Dash-dot line denotes the synchronized-leg-swimming kinematics trajectory and the solid line indicates the alternating-leg-swimming kinematics trajectory. The insect will have reached steady state by $y=15$ cm. The insect's initial positions for the center of mass are $(-2,0)$ and $(2,0)$ for the synchronized- and alternating-leg-swimming kinematics, respectively. The circles indicate the position of the head at each second, with labels indicating time in seconds. (b) Trajectory of head location during two swims of a *H. piceus* beetle from Hughes (1958). Insect swam from bottom to top of the figure, as indicated by the arrow. Labeled markers along path indicate the instant the hind legs begin to retract, where L_3 indicates the left hind leg and R_3 the right.

reduced forward velocity peak-to-peak amplitude of 0.46 cm s^{-1} which is consistent with the more sustained \tilde{a}_y from Fig. 4(b). The mean U_y for the synchronized- and alternating-leg-swimming kinematics are 6.18 and 5.89 cm s^{-1} , respectively, with the velocity magnitude, $|\tilde{U}|$, of the alternating-leg-swimming kinematics equaling 5.91 cm s^{-1} . From Fig. 4(c) it is also clear that $\langle \tilde{\omega}_z \rangle \approx 0$ as well as $\langle \tilde{v}_x \rangle \approx 0$ thus showing that the initial conditions $\omega_{z,0}$ and $\theta_{z,0}$ have resulted in the insect swimming straight in the time-averaged sense at steady state, as specified in Section 2.2.5.

The calculated hydrodynamic efficiencies for the two modes of swimming are 18% and 13% for the synchronized- and alternating-leg-swimming kinematics, respectively. The relative improvement in hydrodynamic efficiency for synchronized-leg-swimming kinematics is 39% compared to the alternating-leg-swimming kinematics.

3.1. Parameter study

A parameter study was also done to determine the relative influence of the various inputs into the system on the beetle's swimming performance, as measured by the hydrodynamic efficiency, η , and average forward velocity, \overline{U}_y . Eight variables were evaluated by individually increasing and decreasing the respective value by $\approx 10\%$. The results of the parameter study are given in Table 1 as the values of η and \overline{U}_y along with the change from the unperturbed case for both the synchronized-leg-swimming and alternating-leg-swimming kinematics. The ratio of the power to recovery stroke length is the length of the power stroke divided by the length of the recovery stroke. It is used to assess the assumption of when along the stroke path to start the power portion of the stroke and when to start the recovery portion. Under the unperturbed conditions the power to recovery stroke length ratio is 1.2 and is

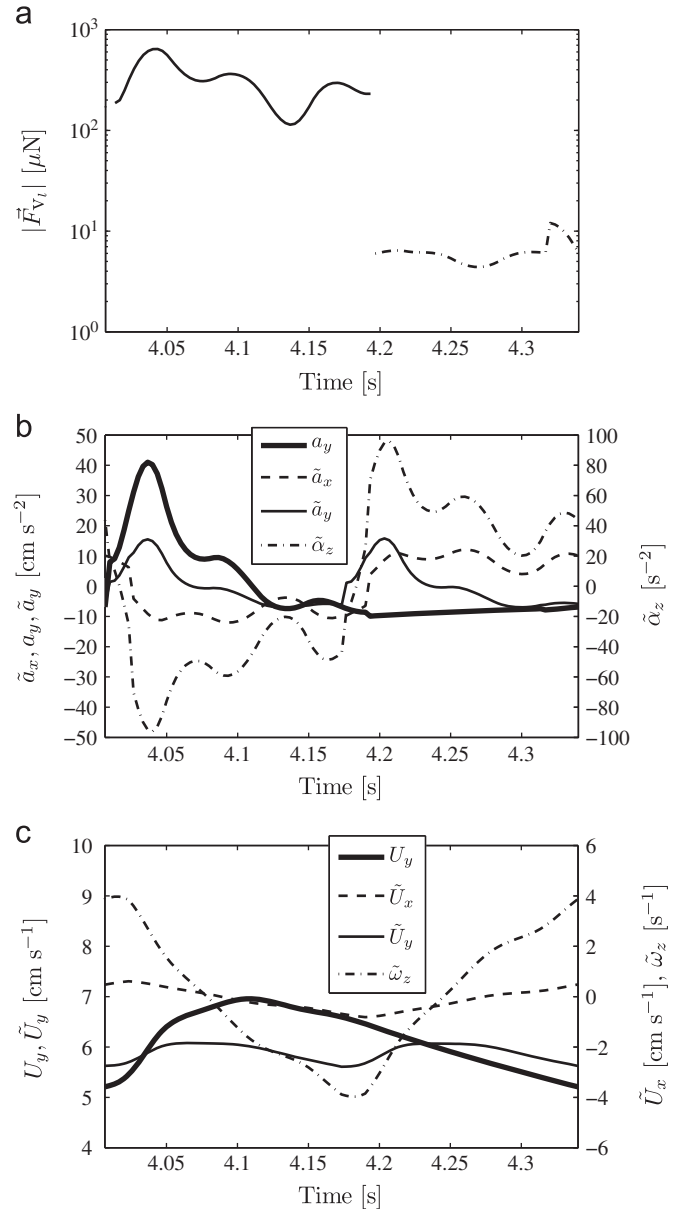


Fig. 4. Plots of the force magnitude from the leg vortices, accelerations, and velocities of the insect during one stroke cycle during steady state swimming. The values of α_x , α_z , U_x , and ω_x are omitted as they are identically zero. Values overmarked with \sim indicate the alternating-leg-swimming kinematics, whereas unmarked values indicate the synchronized-leg-swimming kinematics: (a) semilog plot of the magnitude of the forces from the motion of the left leg during one stroke cycle where the solid line indicates the power stroke and the dot-dashed line indicates the recovery stroke. For synchronized-leg-kinematics, the right leg forces are identical and for alternating-leg-swimming kinematics the right leg forces are offset by half a period. (b) Plot of the translational and angular accelerations with the translational acceleration values given on the left axis and the angular acceleration values given on the right axis. For the alternating-leg-swimming kinematics, the left leg conducts a power stroke and then the right leg, hence the negative then positive angular acceleration. (c) Plot of the translational and angular velocities with the translational acceleration in the y -direction given on the left axis and the translational acceleration in the x -direction and angular acceleration values given on the right axis.

perturbed to ≈ 1.33 and $1.08\bar{3}$ for the 8.46% and -11.36% perturbation amounts, respectively.

4. Discussion

The results of this model of *D. marginalis* swimming agree well with the actual swimming speeds reported in literature.

Table 1

Results from the parameter study with each perturbed variable, the amount of perturbation, and its effect on the synchronized- and alternating-leg-swimming kinematics in terms of the hydrodynamic efficiency, η , and mean forward velocity, \bar{U}_y . The last two columns give the effect on the efficiency improvement for synchronized-leg-swimming kinematics over alternating-leg-swimming kinematics. Columns with “% chng.” give the percentage change in that value from the unperturbed results.

Perturbed variable	Perturbed amount (%)	Sync.-leg-swimming kinematics				Alt.-leg-swimming kinematics				Efficiency improvement	
		η (%)	% chng.	\bar{U}_y (cm/s)	% chng.	η (%)	% chng.	\bar{U}_y (cm/s)	% chng.	$\eta_{sync}/\eta_{alt}-1$	% chng.
Body depth	10.00	17.5	-4.65	5.89	-4.68	12.7	-3.73	5.63	-4.51	38.08	-3.38
	-10.00	19.4	5.32	6.52	5.41	13.8	4.50	6.20	5.26	40.50	2.77
Body length	10.00	18.6	1.02	6.20	0.31	14.2	7.67	5.98	1.48	30.80	-21.86
	-10.00	18.2	-1.00	6.16	-0.32	12.0	-8.85	5.78	-1.88	51.41	30.45
Body width	10.00	17.5	-4.65	5.89	-4.68	12.6	-4.20	5.62	-4.59	38.76	-1.64
	-10.00	19.3	5.31	6.52	5.42	13.9	5.16	6.21	5.37	39.61	0.51
Leg width during power stroke	10.00	20.4	10.84	6.80	10.06	13.6	3.51	6.41	8.81	49.29	25.07
	-10.00	16.4	-10.98	5.56	-10.11	12.5	-5.07	5.35	-9.21	30.73	-22.02
Leg width during recovery stroke	10.00	18.2	-0.81	6.17	-0.17	13.1	-0.88	5.88	-0.22	39.51	0.25
	-10.00	18.5	0.75	6.19	0.15	13.3	0.96	5.90	0.20	39.12	-0.74
Ratio of power to rec. stroke length	8.46 ^a	18.5	0.91	6.24	0.93	13.6	2.82	5.96	1.19	36.82	-6.56
	-7.77 ^a	18.2	-1.05	6.13	-0.90	12.9	-2.45	5.83	-1.09	41.41	5.08
Body mass	10.00	18.3	-0.16	6.19	0.06	13.5	2.66	5.92	0.48	35.59	-9.70
	-10.00	18.4	0.23	6.18	-0.08	12.8	-2.95	5.86	-0.58	43.98	11.59
Beat frequency	10.00	18.4	0.00	6.80	10.00	13.2	0.00	6.48	10.00	39.41	0.00
	-10.00	18.4	0.00	5.56	-10.00	13.2	0.00	5.30	-10.00	39.41	0.00

^a Perturbation does not exactly equal 10% due to numerical discretization and desire to equally perturb from the beginning and end of the power stroke, thus the perturbation magnitudes closest to 10% were used.

Hughes (1958) does not provide a swimming speed for the insect from which the kinematics are derived, however Ribera et al. (1997) reports an average swimming speed of $5.03 \pm 1.35 \text{ cm s}^{-1}$ (mean \pm standard deviation, $N=34$) for *D. marginalis*. Thus the calculated speed of 6.18 cm s^{-1} for the synchronized-leg-swimming kinematics is within one standard deviation of the reported mean value from Ribera et al. (1997) and is within the range of speeds at which an actual *D. marginalis* could swim. Based on the calculated swimming speed and beetle length, a Reynolds number of ≈ 2300 is calculated, thus confirming that the assumed model for circulation growth in Section 2.2.3 is accurate for this modeling. For an insect swimming at a beat frequency of approximately 4 Hz, Nachtigall (1980) reports a swimming speed of 10.4 cm s^{-1} for *D. marginalis* using different leg kinematics than that of this model. Increasing the stroke beat to 4 Hz in the model yields a mean, steady-state velocity of 8.24 cm s^{-1} which is much closer than the swimming speed obtained at 3 Hz.

This model shows that the synchronized-leg swimming of *D. marginalis* is more hydrodynamically efficient than alternating-leg-swimming kinematics by 39%. This confirms the suggestions in the entomological literature over the years (Needham and Williamson, 1907 and Hughes, 1958) that the synchronized-leg-swimming kinematics of many of the *Dytiscidae* family yields a significant increase in swimming efficiency.

The question of synchronized- versus alternating-leg-kinematics has also been addressed previously by the study of frogs, some species of which exclusively swim with alternating-leg-kinematics or transition from alternating- to synchronized-leg-kinematics for swimming (Abourachid and Green, 1999; Nauwelaerts and Aerts, 2002; Johansson and Lauder, 2004). Nauwelaerts and Aerts (2002) showed that alternating-leg swimming yielded lower velocities than synchronized-leg swimming and furthermore suggested that synchronized-leg swimming is relatively more efficient than alternating-leg swimming at higher velocities. This appears to agree with the results presented in the current paper for the swimming beetle *D. marginalis*,

however an exact comparison cannot be made between this study and the frog studies as the frogs did not swim at the same beat frequency in both kinematic modes (Nauwelaerts and Aerts, 2002).

On the other hand, this work is in contrast to a one-dimensional model of krill (*Euphausia pacifica*) swimming by Alben et al. (2010) that reports that alternating-leg-swimming kinematics for two-legged swimming yields a higher swimming velocity even when accounting for the energy expended by each mode of swimming. In particular, since krill are known to conduct diurnal migrations (Mauchline and Fisher, 1969) it seems that krill may have adapted themselves for maximum propulsive efficiency and suggests that metacronal swimming (a wave-like progression of the legs that reduces to simply alternating legs for two legged organisms) would be most efficient, however previous studies of frogs (Nauwelaerts and Aerts, 2002) and the current study on *D. marginalis* report that synchronized-leg kinematics is most efficient. In the current model, if the body rotation is eliminated, then the alternating-leg kinematics performs as well as the synchronized-leg kinematics, suggesting that the loss in efficiency and speed with the alternating-leg kinematics is an issue of body rotation. This is reasonable as frogs and *D. marginalis* exhibit significant back-and-forth body rotations during alternating-leg-kinematics swimming and frogs using alternating-leg-kinematics tend to leave a leg behind them to act as a rudder to help reduce the angular rotations (Abourachid and Green, 1999). This is in contrast to the krill's pleopods (legs) which all contribute to rotational moments of the same sign. Furthermore, krill may use their uropods and telson (tail fan) as a hydrodynamic control surface (much like an airplane's horizontal stabilizer) to help offset the torque from the pleopods. However, for the krill the pleopods all contribute to the same direction of rotation and this, along with the tail fan, may assist the krill in keeping their desired swimming angle (Miyashita et al., 1996).

The parameter study provides insight into particular variables that have a significant effect on the resulting swimming

performance of the beetle. The efficiency improvement between synchronized- and alternating-leg kinematics is always $> 30\%$ indicating that the conclusion of synchronized-leg-kinematics being preferred to alternating-leg-kinematics for *D. marginalis* is robust to significant perturbations $\mathcal{O}(10\%)$. For both the synchronized- and alternating-leg-swimming kinematics, the beat frequency of swimming had a direct effect on the swimming speed, whereas it had no effect on the hydrodynamic efficiency as it equally increases the numerator and the denominator. For the synchronized-leg-swimming kinematics, the hydrodynamic efficiency and average swimming speed are inversely related to the changes in the beetle body cross-section (depth and width). The inverse relation between the beetle swimming performance and the depth and width of the beetle body are due to the force produced by the body vortex, v_b , being directly proportional to the beetle's depth, d_b , and width, w_b , and slowing the beetle down. The other significant perturbation for the synchronized-leg-swimming kinematics is due to the leg width during the power stroke. From Eq. (8), $\bar{F}_{v_i} \sim w_i^2$ indicates that the force from the leg vortex rings is very sensitive to the leg width. This is also seen in Fig. 4(a) as the force magnitude during the power stroke is significantly higher than that during the recovery stroke and thus explains the large magnitude of the dependence of the leg width during the power stroke on swimming performance. The wake-based model presented here also suggests that beetles have increased the width of their legs during the power stroke to increase the force from producing vortex rings—ultimately increasing their hydrodynamic efficiency and swimming speed.

For the alternating-leg-swimming kinematics, the parameter study shows inverse relations between the body cross-sectional area (depth and width) and swimming performance as also seen in the synchronized-leg-swimming kinematics. There also is a positive relation between the leg width during the power stroke and swimming performance, however to a lesser degree due to the significant amount of body rotation. For the alternating-leg-swimming kinematics, the body length, body mass, and ratio of power to recovery stroke length become more significant variables than in the synchronized-leg-swimming kinematics case. The body length is positively related to swimming performance due to its positive relation to the mass moment of inertia and added-mass of the beetle. These both help to reduce the amount of rotation which keeps the beetle moving straighter and thus improves the overall swimming performance. The body mass also directly affects the mass moment of inertia and for the same reasons contributes, to a lesser degree, to improving swimming performance. The ratio of power to recovery stroke length is positively correlated to swimming performance due to increased power stroke length contributing to higher forward velocities while having a lesser effect on the amount of rotation, allowing for an overall increase in the hydrodynamic efficiency.

In general, the parameter study also highlights key variables for modeling this insect: beat frequency, leg width during power stroke, and, to a lesser degree, the body cross-sectional area. The beat frequency was obtained from two papers (Hughes, 1958; Nachtigall, 1980), both of which lack statistics and are simply single observations of an individual's performance. Thus the assumption of 3 Hz for the beat frequency used in the modeling is based on available data. Additionally, as mentioned previously in this section, the beat frequency only has an effect on the swimming speed and not the hydrodynamic efficiency, thus for the purposes of comparing synchronized- to alternating-leg kinematics, it is a non-essential parameter. The leg width during power stroke is the other largely significant parameter and one that was assumed a value from another species. If one considers the leg width during power stroke as a free parameter and aims to match the mean velocity reported in Ribera et al. (1997), then the effective leg width during the

power stroke becomes 3.4 mm compared to the 4.2 mm originally used in the modeling. This reduces the relative improvement in hydrodynamic efficiency for synchronized-leg-swimming kinematics to 25% compared to the original 39%.

The model predicts the motions of a *D. marginalis* beetle with alternating-leg-swimming kinematics. Fig. 3(b) shows the tracing of the insect head of *H. piceus* during swimming that is much like that shown in Fig. 3(a). Sudo et al. (2006) reports on *Guignotus japonicus* Sharp, a diving beetle from the *Dytiscidae* family with a body length of approximately 2 mm (an order of magnitude smaller than *D. marginalis* used in this study) which uses alternating-leg swimming kinematics. The significant angular motion shown in this model is also apparent in the motion of *G. japonicus*, however both *H. piceus* and *G. japonicus* do not have as large of oscillation amplitude as the modeled *D. marginalis* as they swim with their middle legs out of phase of their hind legs to ensure straighter forward motion (Hughes, 1958; Sudo et al., 2006). Thus to correctly model the swimming performance of aquatic insects who use both hind and middle legs with alternating-leg-swimming kinematics, it would be prudent to include the middle leg motion in order to reduce the head track oscillation amplitude. It is expected that the middle legs help balance the torque put on the insect body as it swims—allowing the insect to swim and track its target (prey, mates, etc.) more easily with reduced rotations of its body.

The initial conditions required for the alternating-leg-swimming kinematics proved to be necessary to ensuring straight motion of the insect at steady state. In the real insect it is reasonable to expect that the insect will correct for the issues of torque during start-up by adjusting the breadth or speed of the leg motion. This is because *D. marginalis* and other swimming insects (both synchronized- and alternating-leg swimming) are able to adapt their stroke kinematics in order to turn while swimming as seen in the asymmetric paths of Fig. 1(b) (Hughes, 1958). It would be of interest to capture the motion of *D. marginalis* and other aquatic insects starting from rest to determine whether this hypothesis is true.

The assumption for the leg kinematics in Section 2.1.1 is that the observed stroke path of the right leg was the correct path whereas the left leg was controlled for turning. To verify this assumption, the model was changed to use the left leg kinematics. This yielded hydrodynamic efficiencies of 22% and 19% for the synchronized- and alternating-leg-swimming kinematics, respectively, and a relative efficiency improvement of 15% for synchronized- over alternating-leg swimming. This is a significant reduction in improvement from the original assumption, however the conclusion that synchronized-leg swimming for *D. marginalis* is more hydrodynamically efficient remains the same. The model also assumes that the legs are a straight line from the hind coxae to the leg tip (Section 2.1.2) and, as mentioned, this assumption is not as accurate during the recovery stroke due to leg bending. However, based on Fig. 4(a), it is clear that the magnitude of the forces during the recovery are significantly less than during the power portion of the stroke and thus correcting this assumption would have a negligible effect on the overall swimming performance.

Another assumption that needs to be further addressed is the wake structure of this model. In particular, the wake is assumed to be parallel to the leg at all times. This is not seen in experiments toward the end of the power stroke as the forming vortex is shed downstream as the flat plate comes to a stop (Kim, 2010). However, as mentioned, the effect of the vortex decays quickly (r^{-2}) and thus this may be of little consequence. For the synchronized-leg swimming, the legs perform what appears to be similar to a 'clap' mechanism and Kim (2010) shows that this will produce a single downstream vortex from the two leg vortices. In the Dwarf African frog, *Hymenochirus boettgeri*, this 'clap' mechanism has been suggested to produce a central jet to greatly enhance propulsion (Gal and Blake, 1988). However Johansson and Lauder (2004), studying swimming in

the Northern Leopard frog, *Rana pipiens*, found no central jet at the end of their synchronized-leg-kinematic power stroke, although Richards (2010) suggests that this may be a species-specific effect. Thus it would be necessary to verify this experimentally before considering its inclusion in a model as it is not known whether *D. marginalis* exhibits this ‘clap’ and central jet during swimming.

Acknowledgments

The author thanks Professor J.O. Dabiri and K. Sutherland for their helpful discussions and comments on this work. The author also thanks the reviewers of this paper for their helpful feedback and suggested additions to make this a better paper.

References

- Abourachid, A., Green, D.M., 1999. Origins of the frog-kick? Alternate-leg swimming in primitive frogs, families leiopelmatidae and ascaphidae. *J. Herpetol.* 33 (4), 657–663.
- Achenbach, E., 1974. Vortex shedding from spheres. *J. Fluid Mech.* 62, 209–221.
- Alben, S., Spears, K., Garth, S., Murphy, D., Yen, J., 2010. Coordination of multiple appendages in drag-based swimming. *J. R. Soc. Interface* 7 (52), 1545–1557.
- Brennen, C.E., 1982. A Review of Added Mass and Fluid Inertial Forces. Technical Report. Department of the Navy, Port Hueneme, CA, USA.
- Gal, J.M., Blake, R.W., 1988. Biomechanics of frog swimming ii. Mechanics of the limb-beat cycle in *hymenochirus boettgeri*. *J. Exp. Biol.* 138, 413–429.
- Giovannina, M.V.D., Pirisinua, Q., Giangiuliania, G., Gorettia, E., Pampanella, L., 1999. Oxygen consumption in two aquatic coleoptera species: *Hydrous piceus* and *dytiscus marginalis*. *Ital. J. Zool.* 66 (4), 329–332.
- Hughes, G.M., 1958. The co-ordination of insect movements iii. Swimming in *dytiscus, hydrophilus*, and a dragonfly nymph. *J. Exp. Biol.* 35 (3), 567–583.
- Johansson, L.C., Lauder, G.V., 2004. Hydrodynamics of surface swimming in leopard frogs (*rana pipiens*). *J. Exp. Biol.* 207, 3945–3958.
- Kim, D., 2010. Characteristics of Three-Dimensional Vortex Formation and Propulsive Performance in Flapping Locomotion. Ph.D. Thesis. California Institute of Technology.
- Mauchline, J., Fisher, L.R., 1969. The biology of euphausiids. *Advances in Marine Biology*, vol. 7. Elsevier.
- Miyashita, K., Aoki, I., Inagaki, T., 1996. Swimming behavior and target strength of isada krill (*euphausia pacifica*). *ICES J. Mar. Sci.* 53 (2), 303–308.
- Nachtigall, W., 1980. Mechanics of swimming in water-beetles. *Aspects of Animal Movement*. No.5 in Society for Experimental Biology—Seminar Series. University of Cambridge, Ch, pp. 107–124.
- Nachtigall, W., Bilo, D., 1974. Hydrodynamics of the body of *Dytiscus Marginalis* (Dytiscidae, Coleoptera). In: *Swimming and Flying in Nature*. Plenum Publishing Corporation, Ch, pp. 585–595.
- Nauwelaerts, S., Aerts, P., 2002. Two distinct gait types in swimming frogs. *J. Zool.* 258, 183–188.
- Needham, J.G., Williamson, H.V., 1907. Observations on the natural history of diving beetles. *Am. Nat.* 41 (488), 477–494.
- Ribera, I., Foster, G.N., Holt, W.V., 1997. Functional types of diving beetle (coleoptera: Hydrobiidae and dytiscidae), as identified by comparative swimming behavior. *Biol. J. Linn. Soc.* 61, 537–558.
- Richards, C.T., 2010. Kinematics and hydrodynamics analysis of swimming anurans reveals striking inter-specific differences in the mechanism for producing thrust. *J. Exp. Biol.* 213, 621–634.
- Ringuette, M.J., Milano, M., Gharib, M., 2007. Role of the tip vortex in the formation of low-aspect-ratio flat plates. *J. Fluid Mech.* 581, 453–468.
- Rosenhead, L. (Ed.), 1963. *Laminar Boundary Layers*. Oxford University Press.
- Sudo, S., Yano, T., Kan, Y., Yamada, Y., Tsuyuki, K., 2006. Swimming behavior of small diving beetles. *J. Adv. Sci.* 18 (1&2), 46–49.
- Thomson, J.J., 1883. *A Treatise on the Motion of Vortex Rings*. MacMillan and Co.